Scaling unreinforced masonry for reduced-scale seismic testing

S. Petry & K. Beyer

Bulletin of Earthquake Engineering
Official Publication of the European Association for Earthquake Engineering

ISSN 1570-761X
Volume 12
Number 6

Bull Earthquake Eng (2014)
12:2557-2581
DOI 10.1007/s10518-014-9605-1

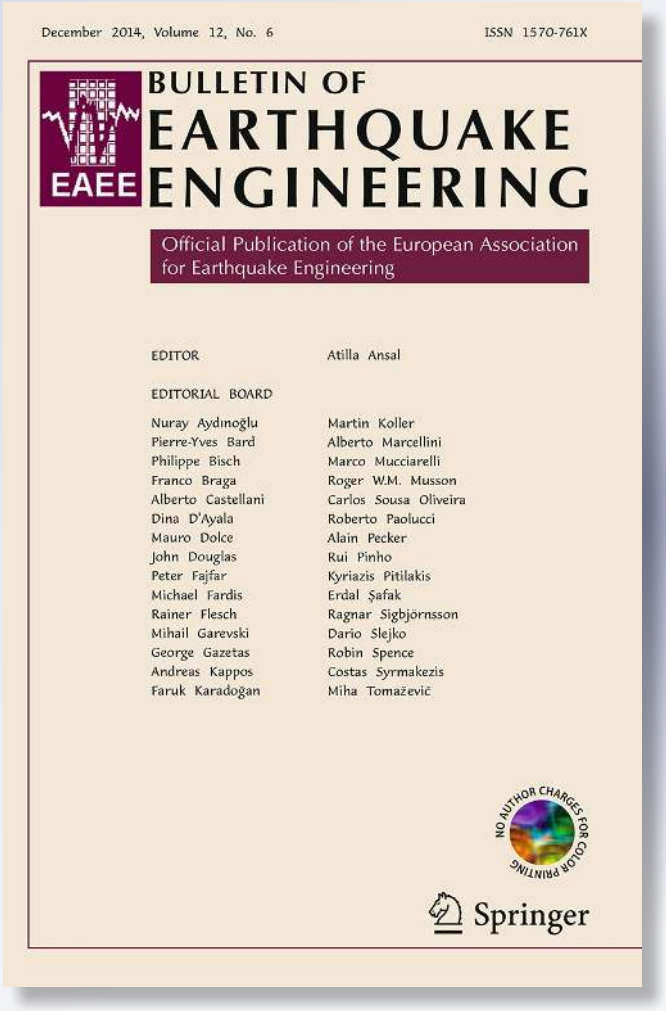

Springer

Bull Earthquake Eng (2014) 12:2557–2581
DOI 10.1007/s10518-014-9605-1

ORIGINAL RESEARCH PAPER

Scaling unreinforced masonry for reduced-scale seismic testing

S. Petry · K. Beyer

Received: 23 August 2013 / Accepted: 2 March 2014 / Published online: 14 March 2014

Abstract When testing multi-storey structures, most testing facilities require the testing of a reduced-scale model. A literature review on tests of scaled masonry structural components revealed that scaling of masonry was rather challenging and often significant differences in stiffness, strength and failure mechanisms between the different sized masonry were reported. This paper addresses the scaling of hollow clay brick masonry with fully mortared head and bed joints. We investigate different choices of scaling brick units and mortar joints. Based on the results of an extensive test programme including standard material tests and quasi-static cyclic tests on masonry walls subjected to horizontal and axial loads, we formulate recommendations for the production of a half-scale model of unreinforced masonry structures. The experimental results show a good match between full-scale and half-scale masonry. We discuss the differences in material properties that remained and compare the force-displacement hystereses obtained for the wall tests.

Keywords Unreinforced masonry · Small-scale testing · Displacement capacity · Force capacity · Mechanical properties

1 Introduction

A general problem in experimental testing of civil engineering structures relates to the required size of the test unit: the examined structures are normally of such large dimensions

S. Petry
Earthquake Engineering and Structural Dynamics Laboratory (EESD), School of Architecture, Civil and Environmental Engineering (ENAC), École Polytechnique Fédérale de Lausanne (EPFL), GC B2 415, Station 18, 1015 Lausanne, Switzerland
e-mail: sarah.petry@epfl.ch

K. Beyer (✉)
Earthquake Engineering and Structural Dynamics Laboratory (EESD), School of Architecture, Civil and Environmental Engineering (ENAC), École Polytechnique Fédérale de Lausanne (EPFL), GC B2 504, Station 18, 1015 Lausanne, Switzerland
e-mail: katrin.beyer@epfl.ch

(buildings, bridges, etc.) that it is usually impossible to test entire structures at full-scale. As a consequence, either only parts of the whole structure are tested or the test units are model structures which are scaled down to a size that can be accommodated in the testing facility. The latter is typically required for shake table tests of multi-storey structures. With respect to the scaling of unreinforced masonry structures, the results reported in the literature are inconclusive: While some early works report a good similitude with regard to the global behaviour of URM panels at different scales (Sinha and Hendry 1969; Hendry and Sinha 1971) more recent works on scaling of masonry reported unsatisfactory similitude of stiffness, strength and failure mechanisms (e.g. Egermann et al. 1991; Abrams 1996). All reports in the literature relate to the scaling of solid brick masonry.

The aim of this article is to provide recommendations for the scaling of bricks and mortar joints for hollow clay brick masonry. When dealing with seismic tests, the model masonry at half-scale should behave as similar as possible as the prototype masonry when subjected to axial and horizontal loads. The similitude should extend to stiffness, strength, hysteretic behaviour, failure mode and deformation capacity of the masonry. This study was conducted as preparation for a shake table test on a modern 4-storey building with reinforced concrete and unreinforced masonry walls.

Since the scaling of hollow clay brick masonry has not been discussed in the literature before, our investigation builds on the findings of studies on the scaling of solid clay brick masonry, which was investigated in several research projects. We modify these where required and address also questions that are specific to the scaling of hollow clay brick masonry such as for example the scaling of web and shell thicknesses of the brick. Furthermore, most previous investigations addressed the similarity of small-scale and full-scale masonry on the basis of force-based tests on material components and small masonry assemblies. With the introduction of performance-based design, the focus of seismic tests lies next to the strength also on the deformation capacity of the structure. For this reason, studies on the scale effect need to address the similitude with regard to the entire force-displacement response up to failure. To do so, we conduct besides standard material tests quasi-static cyclic tests at full- and half-scale and compare stiffness, strength, hysteretic energy, deformation capacity, crack widths and failure mode.

This article commences with a review of studies on the scaling of solid clay masonry (Sect. 2). Based on these findings and own tests on hollow clay brick masonry, guidelines for the scaling of the brick unit and the mortar joint are proposed (Sect. 3). The resulting model masonry is compared to the prototype masonry through standard material tests (Sect. 4) and quasi-static cyclic tests on walls (Sect. 5). Section 6 concludes on the main points that need to be considered when developing hollow clay brick masonry for small-scale testing.

2 Scaling of masonry: literature review

According to Tomaževič, three similarities are important for obtaining a good similitude in the overall behaviour of reduced-scale and full-scale masonry structures (Tomaževič 1987): (i) the similarity in failure mechanism, (ii) the similarity of stresses and (iii) the similarity in mass and stiffness. The similarity in failure mechanism is important for a correct simulation of energy dissipation. The type of failure mechanism that forms depends on shear and axial stresses acting on the masonry, which in a dynamic test are controlled by the mass and the dynamic properties of the structure. The following sections outline the scaling laws for dynamic tests on small-scale specimens, the effect of scaling on the mechanical properties of

Table 1 Scaling laws for an artificial mass simulation (Krawinkler 1979)

Variable	Scaling	Variable	Scaling
Length	S_l	Strain	1
Time	$\sqrt{S_l}$	Stress	1
Frequency	$1/\sqrt{S_l}$	Strength	1
Velocity	$\sqrt{S_l}$	E-modulus	1
Gravity	1	Displacement	S_l
Acceleration	1	Force	S_l^2
Mass density	1	Moment	S_l^3

masonry and the approaches documented in the literature aiming at reducing the differences in mechanical properties between small and full-scale masonry.

2.1 Dimensional analysis for a masonry specimen

Several theoretical scaling laws exist, which describe the ideal relationship between different physical properties that are affected by the scaling (e.g. Krawinkler 1979; Tomaževič and Velechovsky 1992). For the scaling of masonry structures, the Artificial Mass Simulation scaling law is typically applied (Krawinkler 1979). This scaling law requires that the reduced-scale masonry has the same mechanical properties (density, stiffness, strength, drift capacity) as the full-size masonry. Attempts in the past to apply scaling laws to masonry that require a modification of the small-scale masonry properties and therefore the usage of different materials for the brick at small- and full-scale led often to a compromise between required mass and strength of the model material. Poor similitude in the behaviour of the model and prototype masonry allowed only a qualitative comparison of the seismic response of model and full size structure (Tomaževič 1987).

When applying the Artificial Mass Simulation scaling law, the density of the material at reduced- and full-scale is the same. If the length is divided by a factor of S_l, the area reduces by S_l^2. Since the gravity forces are related to the volume (S_l^3) and the gravitational constant g remains unaltered, a mass equal to $(S_l - 1)$ times the mass of the scaled structure has to be added in order to guarantee equal stresses due to gravity loads. As previously noted, equal vertical stresses are essential for obtaining a similar behaviour at small- and full-scale. In order to obtain also equal horizontal accelerations and therefore shear stresses, the time has to be scaled by $\sqrt{S_l}$ since the displacements are S_l times smaller at small-scale than at full-scale. The resulting scaling laws for the Artificial Mass Simulation are summarized in Table 1.

2.2 Scaling effects on the mechanical properties of solid clay brick masonry

As outlined in the previous paragraph, applying the Artificial Mass Simulation scaling law requires that small- and full-scale masonry have the same mechanical properties, i.e. in particular the same density, stiffness, strength and deformation capacity. While the scaling of hollow clay brick masonry has not been adressed in the literature, scaling of solid clay brick masonry has been the subject of several research projects. This section summarises the findings from studies on scaled solid clay brick masonry while the following sections (Sects. 2.3, 2.4) outline different attempts documented in the literature that aim at modifying the model bricks and joints in order to minimize these differences.

2.2.1 Compressive strength of masonry

The most recent detailed experimental study on scaling of solid clay brick masonry is presented by Mohammed (2006) and Mohammed and Hughes (2011) which comprises different standardised material tests at different scales (1/6-, 1/4-, 1/2- and full-scale). When comparing the results of compression tests, similar failure patterns were observed for the specimens at all scales. Despite this, the compressive strength was significantly higher for the masonry panels tested at 1/6- and 1/4-scale than the compressive strength of the full-scale masonry. The 1/2-scale masonry developed a compressive strength similar to the full-scale masonry. This is in agreement with the findings by previous studies (e.g. Hendry and Murthy 1965), which also found an increased compressive strength for small-scale masonry.

The increase in strength was attributed to the following two phenomena: (1) the burning of a reduced-scale brick can lead to an increased brick strength (Egermann et al. 1991) and (2) the scaling of the mortar joint affects the percentage of water sucked from the mortar by the brick during the curing of the mortar and thus the strength of the mortar joint (Drysdale and Hamid 2008; Mohammed and Hughes 2011). Mohammed (2006) reported that the brick unit at 1/6- and 1/4-scale was indeed slightly stronger in compression than the prototype brick. Nevertheless, the brick strength at different scales varied less than the masonry strength and it was therefore concluded that both phenomena contribute to the difference in compressive strength between full-scale and small-scale masonry. One alternative could be to scale only the width of the bricks but neither length, nor height of the brick nor the thickness of the mortar joints. However, Hamid et al. (1986) showed that the compressive strength is related to the number of the brick courses and also Frumento et al. (2009) noted that walls with less courses yielded different results when subjected to lateral loading due to the larger restraint provided by the beams at the top and bottom. Therefore, the scaling of brick size and mortar joint thickness is recommended.

2.2.2 Axial stiffness of masonry

Other researchers reported that the scaling affects also the axial stiffness due to the different overburden stresses during construction (Hendry and Murthy 1965; Egermann et al. 1991). Since the additional masses required by the Artificial Mass Simulation scaling law are typically only installed after the construction of the entire structure has been completed, the compressive stresses acting on the bed joints during curing of the mortar of the small-scale masonry are only half of those of the full-scale masonry. To avoid the difference in overburden stresses, Mohammed and Hughes (2011) built their specimens horizontally and obtained from compression tests similar stiffnesses in the elastic range for the small- and full-scale masonry. While such a construction practice is feasible when conducting material tests on small specimens, it is not possible to construct entire shake table test units in a horizontal position nor does this construction practice reflect the stiffness of real masonry structures. Such an approach is therefore valid for investigating the effect of different parameters on the scaling but cannot be part of recommendations for the construction of scaled test units for shake table tests.

2.2.3 Shear behaviour of masonry

Although scaling of unreinforced masonry structures is particularly relevant for shake table testing, most research projects on scaling investigated chiefly masonry panels subjected to

vertical loads and not to horizontal loads. Exceptions are (i) the study by Benjamin and Williams (1958) who investigated the scale effect on the shear strength of infill masonry walls with concrete frames; (ii) the study by Sinha and Hendry (1969) and Hendry and Sinha (1971) who compared the shear behaviour of masonry panels at full- and reduced-scale, (iii) the study by Abrams (1996) who compared the behaviour of a 2-storey URM building at full- and reduced-scale when subjected to lateral loading; and (iv) the study by Mohammed and Hughes (2011) who studied the influence of the scaling on the masonry shear strength through triplet tests and diagonal compression tests.

In the first study, Benjamin and Williams (1958) tested one storey, single bay RC frames with masonry infills with solid bricks. They compared models at different scales up to 1:4 to prototype specimens. Infills at all scales were constructed using the same solid brick type and the width of the walls was varied by changing the orientation of the bricks. As a result, the number of brick layers changed between scales. According to the literature (e.g. Hamid et al. 1986; Drysdale and Hamid 2008), changing the number of layers affects the shear strength of the masonry and thus a comparison of the models and prototypes is somewhat questionable. Furthermore, as reported by Benjamin and Williams (1958), the scatter of the results within each test series was so significant that a clear trend with the scaling factor could not be identified.

Sinha and Hendry (1969) and Hendry and Sinha (1971) compared full-size URM panels with and without openings with experiments on 1/6-scale panels. The panels were first subjected to a uniform axial compression and then to a lateral monotonic load. Generally, they observed a good agreement between the behaviour of prototype and model panels and only with regard to the post peak behaviour, the model panels tended to have an increased displacement capacity. While the compression strength reported in Sinha and Hendry (1969) and Hendry and Sinha (1971) is similar for both model and prototype brick, this study misses further discussion on the differences between both masonries at full- and 1/6-scale, e.g. surface properties of the model brick, thickness of mortar joints.

Abrams (1996) compared the lateral behaviour of a reduced-scale 2-storey URM building tested dynamically with a test performed on an equivalent structure at full-scale subjected to quasi-static cyclic loading. Since the test type varied between both tests, a comparison was difficult and Abrams (1996) associated most differences to the different loading histories.

In the last study (Mohammed and Hughes 2011), the model bricks were cut after the burning from prototype bricks leading to a smaller surface roughness when compared to the prototype brick that were wire-cut before the burning. As a result, Mohammed and Hughes (2011) observed for the shear triplet tests on full-size masonry a significant higher cohesion and friction than for the model masonry. For the shear triplet tests on the three model masonries, an increase in initial shear strength and a decrease in friction coefficient were observed with increasing scaling factor. Concerning the diagonal compression test, on the contrary, no significant difference between the four scales was observed. Concerning the effect of the scaling on the deformation capacity, Mohammed and Hughes (2011) observed a slight increase in post peak deformation capacity for reduced-scale specimens when tested in diagonal compression; unfortunately a similar statement with regard to the shear deformation capacity obtained from triplet tests is missing.

2.3 Producing solid clay brick units for model masonry

Model bricks are typically produced using the clay from the same pit and applying the same burning procedure as for the prototype bricks. As outlined above, the resulting model brick tends to be stronger than the prototype brick. Different approaches for reducing the difference

in brick strength are reported in the literature. These can be grouped as follows: (i) using a different brick material for the model brick, (ii) reducing the burning temperature for the model brick, or (iii) cutting the model brick from a prototype brick after the burning.

Tomaževič (1987) showed that using a different material for the model brick proved to be too complicated and should be avoided, since not only the brick strength but also the brick density, stiffness and deformation capacity need to be matched. Egermann et al. (1991) experimented with a reduced burning temperature for producing solid clay model bricks but could not obtain a perfect match for the resulting compression strength of the brick. Tomaževič et al. (1990) reported good experiences with the use of model bricks cut after the burning from prototype bricks. Nevertheless, some differences might still be present: Mohammed (2006) noticed for solid bricks the importance of the orientation of the model brick within the original brick, which was also observed by Shrive and Jessop (1980). Also the roughness of the cut surface should be considered (Davies et al. 1995; Mohammed and Hughes 2011) since it determines the shear resistance of the mortar-brick interface.

2.4 Reducing scaling effects on mortar joint properties

In the model masonry the mortar joints have a smaller thickness than in the prototype masonry. The sucking behaviour of the bricks is the main mechanism that affects the properties of the mortar and the joint-brick interface in solid clay brick masonry. The literature reports that for thinner joints the suction of the brick has a larger effect on mortar and interface properties (e.g.Drysdale and Hamid 2008). Due to the suction, the water-cement ratio of the mortar is changed and the crystallization process in the mortar modified. It is, however, difficult to quantify this effect. If the water-cement ratio is only slightly reduced, the strength in the mortar tends to increase. If it reduces significantly, not enough water might be left for the mortar to crystallise completely and the mortar strength might reduce rather than increase. Hence, dependent on the amount of water absorbed by the brick and the initial water-cement ratio of the mortar, the strength of the masonry will either increase or decrease (Mohammed 2006).

Several researchers investigated parameters that could help to control the reduction of the water-cement ratio in the mortar due to the suction process. Brocken et al. (1998) investigated the effect of pre-wetting the bricks but found that this affects the suction process only in a significant manner, if the water content of the brick reaches nearly saturation. They also studied the use of water retention products but concluded that the addition of water retention products does not influence significantly the quantity of water extracted, but only slows down the suction (Brocken et al. 1998). Also Green et al. (1999) mentioned that only very large quantities of water retention products would show significant changes in the amount of water absorbed by the bricks—which could even for small-scale test units become eventually too costly.

3 Scaling hollow clay brick masonry

The objective of this project is to develop a half-scale masonry with hollow clay brick units that has very similar properties as the corresponding full-scale masonry. The behavior of modern masonry with hollow clay brick units is strongly influenced by the anisotropy of the bricks. Hence, when scaling such masonry not only the points outlined for solid brick masonry need to be considered but it is also important to maintain the anisotropy of the units.

3.1 Producing hollow clay brick units for model masonry

Modern hollow clay brick units are produced by extruding a clay strand through a form. Producing a new form for a model brick is rather expensive; moreover at the start of this project we did not know which characteristics this form should have. After discussions with several manufacturers we decided to take the form of an existing brick unit and adapt the outer dimensions of the brick by covering parts of the form; the latter can be done relatively easily. The following paragraphs summarise our considerations when developing a half-scale hollow clay brick unit.

The vertical compressive strength of hollow clay brick units is mainly influenced by the net area of the brick (Ganz 1985). While the shape of the perforation is not decisive for the vertical strength, it has a significant influence on the compressive strength parallel to the bed joints (in the following referred to as horizontal strength). Lourenço et al. (2010) showed that the horizontal compressive strength of bricks with continuous and straight webs and shells was significantly higher than for bricks with rice-shaped holes. When scaling hollow clay brick units it is therefore important to maintain the ratio of net to gross area and to choose a model brick that has a similar hole layout as the prototype brick. The hole layout of a brick can be scaled in two different ways, both respecting the similarity of the void ratio, of the effective width (defined as the net width of the brick) and the hole layout: (i) the geometry is scaled completely, including web and shell thicknesses, or (ii) shell and web thicknesses remain identical and the number of webs is decreased.

After testing several potential model bricks, we opted for a model brick which shell and web thicknesses were similar to those of the prototype brick unit. This yielded the best match of model and prototype brick with regard to the strength of the bricks. Note that this observation is also in good agreement with recommendations given by Eurocode 6 (CEN 2005), which classifies the robustness of masonry bricks according to void ratio, minimum thickness of web and shells and effective width of bricks. With the chosen model brick, all three parameters matched rather well between model and prototype brick. We assume further that the good similitude is based on the following phenomenon: While for solid bricks the development of the temperature in the center of the brick depends on the total size of the brick, for hollow clay bricks the web and shell thicknesses rather than the brick size are decisive. Keeping the web and shell thicknesses identical is therefore advantageous, because it allows the same drying and burning procedure to be used for the model brick as for the prototype brick. Scaling the web and shell thickness rather than reducing the number of webs and shells led also to a reduced strength and a very brittle behaviour of the brick. The final choice of model brick for the prototype brick of this study is shown in Fig. 1 and the mechanical properties of both bricks are summarized in Table 2. Small differences remained with regard to the void ratio and effective width. When loaded perpendicular to the perforation, the model brick was therefore slightly stronger than the prototype brick.

3.2 Mortar for model masonry

The mortar joints of both masonries were fully filled using the cement-based mortar WEBER MUR MAXIT 920. It is one of the most commonly used mortars in Switzerland. The thickness of the joints of the model masonry was scaled. For the full-scale masonry, the measured mortar joint thickness varied between 10 and 12 mm and for the half-scale masonry between 5 and 7 mm. For both types of masonry, head and bed joints had the same thickness and were fully filled. As a result of the different joint thicknesses, the suction process described in the literature review led to a smaller effective water-cement ratio of the mortar for the model

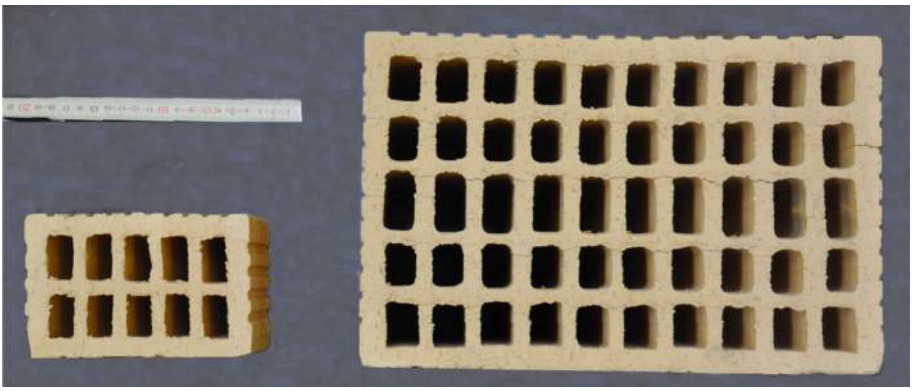

Fig. 1 Final half-scale and full-scale brick from Morandi Frères SA, Switzerland

Table 2 Mechanical and geometrical properties of all investigated bricks (resulting material strength in bold)

	Full-scale brick	Half-scale brick	Ratio half- / full-scale
Average dimensions of a brick			
Length (mm)	**297**	**148**	–
Width (mm)	**194**	**96**	–
Height (mm)	**189**	**94**	–
Average mass and density of a brick			
Mass / brick (kg)	**9.9**	**1.3**	–
Volumetric mass (kg/m^3)	**901**	**996**	1.10
Void ratios and effective length / width of a brick			
Void ratio (%)	**49.3**	**39.5**	0.80
Effective length[a] (%)	**30.6**	**37.8**	1.24
Effective width[a] (%)	**28.9**	**36.5**	1.26
Average strength and deviation			
Compression, parallel to perforation (MPa)	**35.0** $\pm$ 7 %	**33.3** $\pm$ 25 %	0.95
Compression, perpendicular to perforation (MPa)	**9.4** $\pm$ 8 %	**10.8** $\pm$ 17 %	1.15
Flexural tensile strength, perpendicular to perforation (MPa)	**1.27** $\pm$ 38 %	**1.61** $\pm$ 41 %	1.27

[a] The effective length / width describe the percentage of filled material to voids over the gross length / width

masonry than for the prototype masonry. The literature review showed that neither adding water retention products to the mortar nor saturating fully the brick proved to be an ideal option for modifying the properties of the mortar for the model masonry. Own compression tests with different water retention products and pre-wetting of the bricks confirmed these results. Thus, it was decided to construct the half-scale masonry using the same mortar recipe as for the prototype masonry. As discussed in Sect. 2.4, measures such as constructing the masonry horizontally were not considered. In addition, the vertical construction assured a good penetration of the mortar inside the perforation of the brick, which is important for the shear transfer between mortar joint and brick in hollow clay brick masonry.

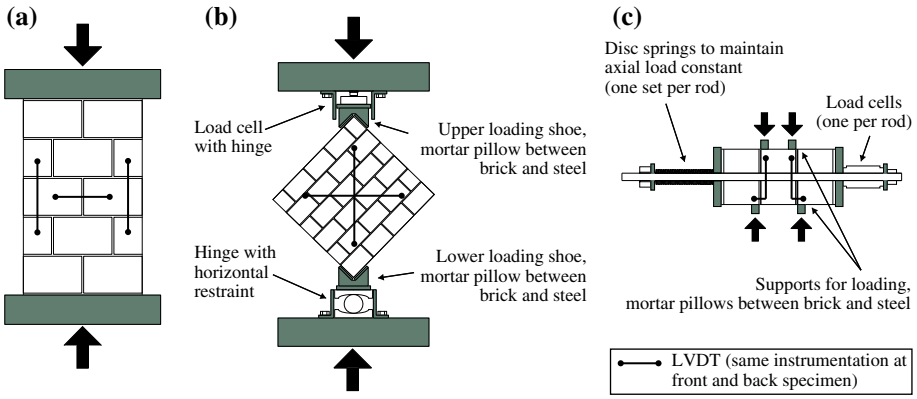

Fig. 2 Material tests performed on half- and full-scale masonry: **a** compression test on masonry wallette, **b** diagonal compression test on square masonry wallette and **c** shear test on masonry triplet

4 Similitude of the material properties of half- and full-scale masonry

Three kinds of material tests were performed on half- and full-scale masonry, i.e. compression tests, shear triplet tests and diagonal compression tests. The different setups for the material tests are illustrated in Fig. 2. The following sections compare the results obtained from these standard tests for the model masonry to those of the prototype masonry.

4.1 Compression tests

For the standard compression test (CEN 2002), a series of five specimens was constructed at each scale. During testing, the deformations of the panels were measured with four vertical and two horizontal LVDTs (Fig. 2). Figure 3 shows the stress-strain curves obtained from the compression tests. For solid brick masonry several researchers had reported an increase in compressive strength for smaller scales, which they attributed partly to the scaling of the brick and partly to the scaling of the mortar thickness (see Sect. 2). In this study, similar strength values were obtained for both brick units (see Table 2). Hence, an increase in masonry strength due to a stronger model brick was avoided and also the scaling of the joint did not affect the compressive strength significantly. As a result, a good match of the compressive strength values was obtained.

The modulus of elasticity E_c was determined as the secant modulus when reaching 1/3 of the maximum stress (CEN 2002). The Poisson's ratio ν was evaluated by comparing the vertical and horizontal strain for the same load point (see position of LVDTs in Fig. 2). While the two types of masonry match perfectly with regard to the Poisson's ratio, the E-modulus of the model masonry is 50 % higher than the E-modulus of the prototype masonry. However, masonry is not isotropic. Thus, the herein determined Poisson's ratio describes the lateral expansion under vertical compression but is not suitable for determining the shear modulus G. In order to compare the E-modulus of model and prototype masonry for larger stress values, the E-modulus is also evaluated comparing the vertical strain and the vertical stress at 1/3 and 2/3 f_u ($E_{1/3-2/3}$, the footnote stands for the stress and strain used, i.e. $\varepsilon_{1/3} = \varepsilon(\sigma = 1/3 f_u)$ and $E_{1/3-2/3} = (2/3 f_u - 1/3 f_u)/(\varepsilon_{2/3} - \varepsilon_{1/3})$), at $2/3 f_u$ and f_u ($E_{2/3-3/3}$) and as secant stiffness at peak strength ($E_{0-3/3}$). The values are summarized in Table 3 and show that for larger stresses the E-moduli of the two types of masonry are rather similar.

Table 3 Results from the compression tests performed on half- and full-scale masonry panels (resulting material strength in bold)

	f_u (MPa)	$E_c = E_{0-1/3}$ (GPa)	E_c/f_u (−)	ν (−)	$E_{1/3-2/3}$ (−) (GPa)	$E_{2/3-3/3}$ (GPa)	$E_{0-3/3}$ (GPa)
Full-scale masonry	**5.87**	**3.55**	**613**	**0.20**	**4.26**	**4.28**	**4.00**
	±5 %	±9 %	±10 %	±19 %	±7 %	±11 %	±8 %
Half-scale masonry	**5.66**	**5.46**	**965**	**0.20**	**4.74**	**4.08**	**4.50**
	±4 %	±8 %	±11 %	±65 %	±11 %	±16 %	±9 %
Ratio half- / full-scale	0.94	1.54	1.57	1.00	1.11	1.05	1.13

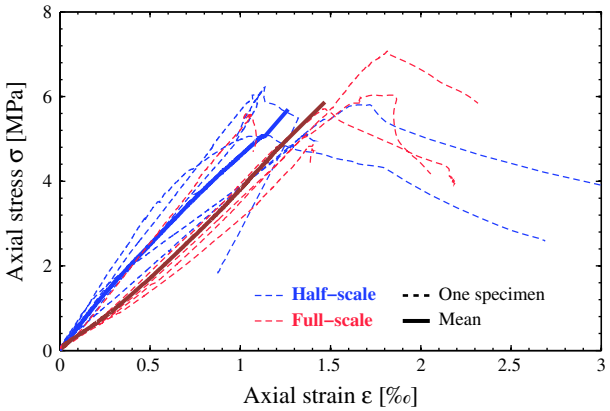

Fig. 3 Stress-strain curves of the compression tests

Figure 3 also shows that the post-peak deformation capacity is subjected to considerable scatter but in average the post-peak deformation capacity of the half-scale masonry is larger for the model masonry than for the full-scale masonry. Lourenço (1997) pointed out that the deformation capacity of masonry failing in compression is affected by size effects, i.e. that reduced-scale masonry possesses a larger deformation capacity than full-scale masonry. The results of the compression tests and the quasi-static cyclic tests on the walls—as will be shown later—confirm this observation.

4.2 Shear triplet tests

Ten shear triplet tests (CEN 2007) were carried out at each scale. The triplets were tested for normal stresses between 0.2 and 0.6 MPa. The friction coefficient μ and the cohesion c characterizing the peak strength were obtained from a best-fit line. The residual shear strength was determined when the shear strength reached for large sliding displacements an approximately constant value. The friction coefficient describing the residual strength regime was obtained from the best fit line passing through the origin (see Fig. 4).

The friction coefficients and the cohesion of the model masonry are approximately 20 % smaller than those of the prototype masonry (Table 4). To the authors' opinion, this discrepancy results from the difference in void ratio of the half- and full-scale brick units (υ_M/υ_P = 0.8, see Fig. 1 and Table 2). Assuming that the shear strength results mainly from the shearing

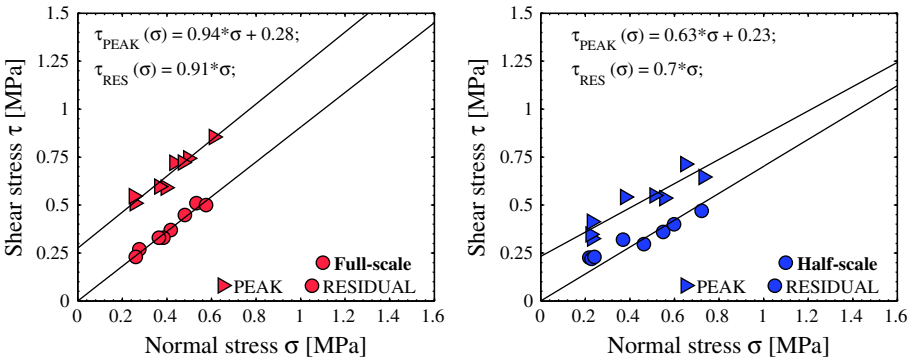

Fig. 4 Results from shear tests on half- and full-scale masonry

Table 4 Results from the shear tests performed on half- and full-scale masonry triplets (resulting material strength in bold)

	c (MPa)	μ (−)
Full-scale masonry	**0.28**	**0.91**
Half-scale masonry	**0.23**	**0.70**
Ratio half- / full-scale	1.18	1.23

off of the mortar pillars, which form when the mortar is pressed inside the voids of the perforated bricks, the shear strength should be proportional to the void ratio. This is confirmed by the shear triplet results. To improve the match of the interface shear strength one should therefore aim for equal void ratios of the half- and full-scale brick unit (Table 4).

4.3 Diagonal compression tests

To determine the diagonal tensile strength, five specimens at each scale were tested under a local compression load at the corners as illustrated in Fig. 2 (RILEM 1991). The lower and upper shoes applying this compression load were scaled with the test unit. Note that no pre-compression perpendicular to the bed joints was applied (Fig. 2). The diagonal tensile strength f_t was computed from the peak force F_{PEAK}:

$$f_t = \frac{F_{PEAK}}{\sqrt{2} \cdot A_N} \tag{1}$$

where A_N represents the average cross section:

$$A_N = \frac{(L \cdot H)}{2} \cdot T \tag{2}$$

where L, H and T are the length, height and thickness of the panel, respectively. The resulting diagonal tensile strengths for the half- and full-scale masonry are summarised in Table 5.

The diagonal tensile strength of the half-scale masonry underestimates the strength of the full-scale masonry by around 30 % ($f_{t,M}$ / $f_{t,P}$ = 0.68). All panels failed along one diagonal crack, which started at the centre of the panels and followed the mortar joint. The diagonal tensile strength was therefore controlled by the joint-brick interface properties. Hence, similar to the shear strength obtained from the triplet tests, the diagonal tensile strength of the model masonry is lower for the model masonry than for the prototype masonry because the void ratio of the model brick unit is lower (see Fig. 5).

Table 5 Results from the diagonal compression tests performed on half- and full-scale masonry panels (resulting material strength in bold)

	L (mm)	H (mm)	f_t (MPa)
Full-scale masonry	1,230	1,190	**0.496** ±9.7 %
Half-scale masonry	615	595	**0.336** ±15 %
Ratio half- / full-scale	–	–	0.68

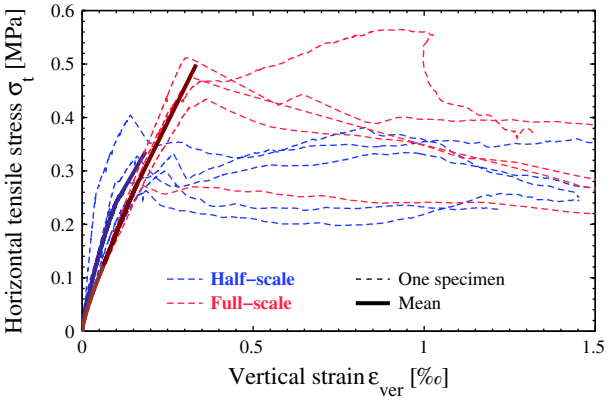

Fig. 5 Stress-strain curves of the diagonal tensile strength

4.4 Summary of differences in material properties

The standard material tests showed that the model masonry agreed well with the prototype masonry with regard to the compressive strength f_u, the axial stiffness E_c and the Poisson's ratio ν. A key factor seems to be the brick strength as the compression failure is associated with the failure of the brick. The model and prototype masonry differed with respect to the deformation capacity of the masonry when subjected to compression. The deformation capacity of the model masonry was 10–50 % larger than the deformation capacity of the prototype masonry.

The shear strength of the brick-mortar interface of the model masonry was ∼20 % less than for the prototype masonry. This was linked to the different void ratios of the model and prototype brick units which could not be avoided since the number of holes but not the web and shell thickness were reduced. The interface properties also governed the tensile strength obtained from diagonal compression tests.

On the whole the correspondence in terms of strength is rather satisfactory while the compression tests indicated that the displacement capacity of the model masonry is larger for the model masonry than for the prototype masonry. This will be investigated further in the next section, which compares the behaviour of half- and full-scale masonry walls subjected to quasi-static cyclic loading.

Table 6 Dimensions and boundary conditions of the quasi-statically tested walls PUM1-5/PUP1-5

Wall unit	H (m)	L (m)	t (m)	H_0/H (−)	N (kN)	σ_0 (MPa)	σ_0/f_u (−)
PUP1	2.225	2.010	0.200	0.5[a]	419	1.04	0.18
PUM1	1.113	1.005	0.100	0.5	105	1.04	0.18
PUP2	2.225	2.010	0.200	0.75	419	1.04	0.18
PUM2	1.113	1.005	0.100	0.75	105	1.04	0.18
PUP3	2.225	2.010	0.200	1.5	419	1.04	0.18
PUM3	1.113	1.005	0.100	1.5	105	1.04	0.18
PUP4	2.225	2.010	0.200	1.5	619	1.54	0.26
PUM4	1.113	1.005	0.100	1.5	124	1.54	0.27
PUP5	2.225	2.010	0.200	0.75	219	0.54	0.09
PUM5	1.113	1.005	0.100	0.75	55	0.54	0.10

[a] For PUP1 a fixed-fixed boundary condition was simulated by applying a zero rotation at the top of the wall. For all other specimens the boundary conditions were simulated in controlling the moment ratio, and thus, the shear span H_0 of the walls

5 Similitude of seismic behaviour of URM walls at half- and full-scale

To investigate the similitude of the model and prototype masonry when subjected to seismic loading, quasi-static cyclic tests on walls were conducted. The following sections outline the test programme, the test setup, the applied loading history and compare the response of the half- and full-scale walls in terms of crack pattern, failure mode and force-deformation characteristics.

5.1 Test programme, test setup and loading history

For the quasi-static cyclic tests, a series of five walls was constructed at each scale using the brick units and mortar that had been used for the material tests. The walls at one scale had all the same dimensions (Table 6) and were tested in the test stands shown in Fig. 6. Each test stand allowed applying two vertical forces and one horizontal force. The control of the three actuators could be fully coupled. For each wall (exception: PUP1, see following section), the applied axial force and the shear span remained constant throughout the test. The horizontal actuator (master) was displacement-controlled. The vertical actuators were force-controlled. The forces to be applied by the two vertical actuators $F_{ver,1,2}$ were computed as a function of the force applied by the horizontal actuator F_{hor} and the axial force N (Fig. 7):

$$F_{ver,1,2} = \frac{N}{2} \pm \mathrm{C} \cdot F_{hor} \tag{3}$$

The constant C is a function of the shear span H_0 and the geometry of the test setup. Figure 7 shows the three different shear spans that were applied in the test series. The walls were subjected to a cyclic loading history with the following peak drifts: 0.025, 0.05, 0.1, 0.15, 0.2, 0.3, 0.4, 0.6, 0.8, 1.0, 1.5, 2.0 %. At each drift level, two cycles of equal amplitude were imposed. The deformations of the walls were measured by an optical measurement system. The average drift of the wall was computed as the horizontal displacement at the top of the wall divided by the wall height H.

A set of conventional hard-wired measurements was used to measure the forces of all three actuators, the global displacement at the top of the wall and the local deformations in

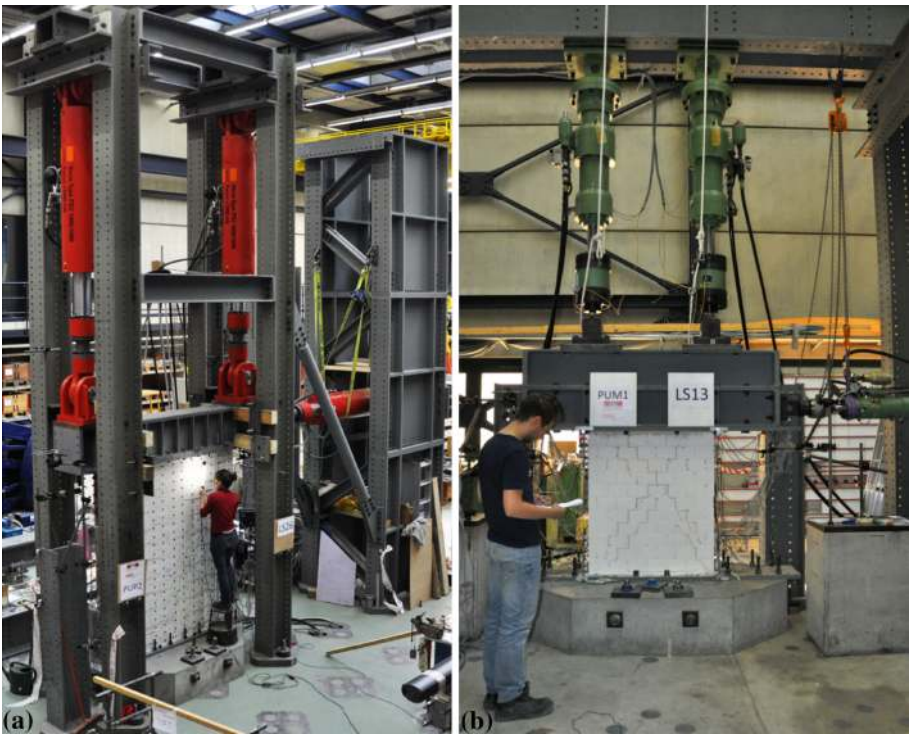

Fig. 6 **a** Photos of test stands for quasi-static cyclic wall tests on prototype walls (PUP1-5) and **b** Model walls (PUM1-5)

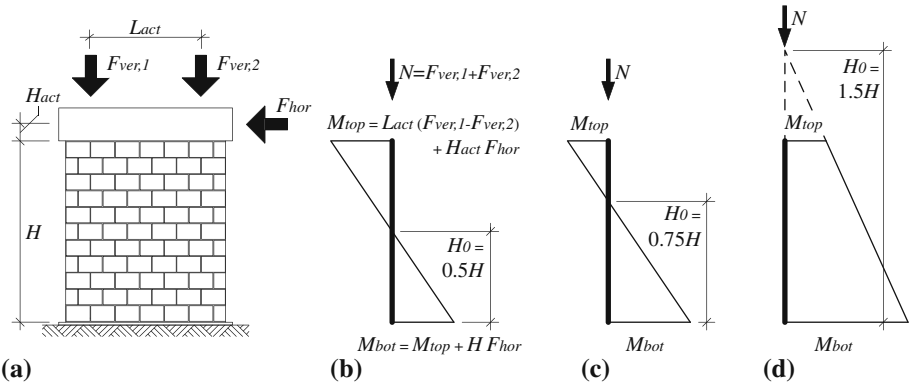

Fig. 7 **a** Boundary conditions for the URM walls at half- and full-scale with the resulting moment profiles for **b** PUM1/PUP1, **c** for PUM2/PUP2 and PUM5/PUP5 and **d** for PUM3/PUP3 and PUM4/PUP4

bricks and joints at all four corners of the wall. In addition, a LED-based optical measurement system was used to follow the displacements of the wall and at the steel plates at the top and bottom of the wall (see markers in Fig. 6a; for the half-scale walls, the markers were fixed on the back of the specimen and are not visible in Fig. 6b).

The test parameters that were varied between the five walls were the applied axial stress and the shear span. Table 6 summarises the test programme and introduces the labels of the wall units for the prototype walls (PUP1-5) and the model walls (PUM1-5). The first three walls were subjected to the same vertical load, while the rotational restraint at the top was varied. For the first wall fixed-fixed boundary conditions were simulated. For the second and third walls the moment applied at the top of the wall was proportional to the applied horizontal load and therefore, the shear span H_0 was constant and equal to 0.75 and 1.5 times the wall height H for the second and third wall, respectively (see Fig. 7). The fourth wall was subjected to the same shear span as the third wall ($H_0 = 1.5H$) but the axial load was increased by ~50 %. The fifth wall was subjected to the same shear span as the second wall ($H_0 = 0.75H$) but the normal load was reduced by ~50 %.

The objective of the research programme was to compare the behaviour of the model and prototype masonry for different performance limit states. For this reason, the quasi-static cyclic loading was continued until the walls were no longer able to carry the applied vertical load. Hence, two different failure limit states are distinct: (i) the "horizontal load failure" refers to the drift where the strength dropped to 80 % of the peak strength; (ii) the "axial load failure" is attained, when the wall could no longer sustain the vertical load applied by the pistons. The first failure criterion—horizontal load failure—corresponds to the limit state "near collapse" (NC) as defined in the Eurocode 8, Part 3 (CEN 2004) and aims at limiting the damage in order to avoid collapse of the structural element. The second failure criterion—axial load failure—would correspond to the collapse or partial collapse of the structure.

5.2 Comparison of crack pattern and failure mode

Pictures of all ten specimens after axial load failure and the hystereses for the half- and full-scale walls are shown in Fig. 8. In order to compare the hysteretic curves of the model and prototype walls, the average shear stress $\tau = V/A$ is plotted against the average drift where A is the gross sectional area of the wall and V the lateral force applied by the horizontal actuator.

All five wall configurations tested at half-scale (PUM1-5) produced similar failure modes and damage patterns as the equivalent full-scale walls (PUP1-5, Fig. 8): PUM1/PUP1, PUM2/PUP2 and PUM5/PUP5 displayed a diagonal shear failure, PUM3/PUP3 a flexural failure and PUM4/PUP4 a hybrid failure mode. In addition, to the failure mechanism also the shape of the hysteresis is well reproduced for all walls resulting thus in similar energy dissipation (Fig. 9). Only for PUM4 and PUP4, the form of the hysteresis differed slightly (Fig. 8) which resulted also in different equivalent hysteretic damping factors (Fig. 9). Both walls failed in a hybrid failure mode and it seems to the authors that it was difficult to reproduce exactly the same behaviour when two failure modes were dominant at the same time. Even though, both walls developed generally the same crack pattern, the hysteretic behaviour of PUM4 resembled more a rocking failure, while the hysteretic behaviour of PUP4 is characteristic for a diagonal shear failure. Accordingly, the equivalent damping obtained for PUM4 was lower than for PUP4.

For PUM1/PUP1, the boundary conditions were imposed slightly differently: PUP1 was tested under fixed-fixed boundary conditions and PUM1 was tested with a constant shear span $H_0 = 0.5H$. Nevertheless, the resulting average shear strength and the drift capacity showed a good similitude (see Fig. 8). For both PUP1 and PUM1 shear cracks started forming during the cycles with a nominal drift of 0.1 %. The peak strength occurred slightly earlier for the model wall than for the prototype wall but the deterioration in the post-peak branch was more

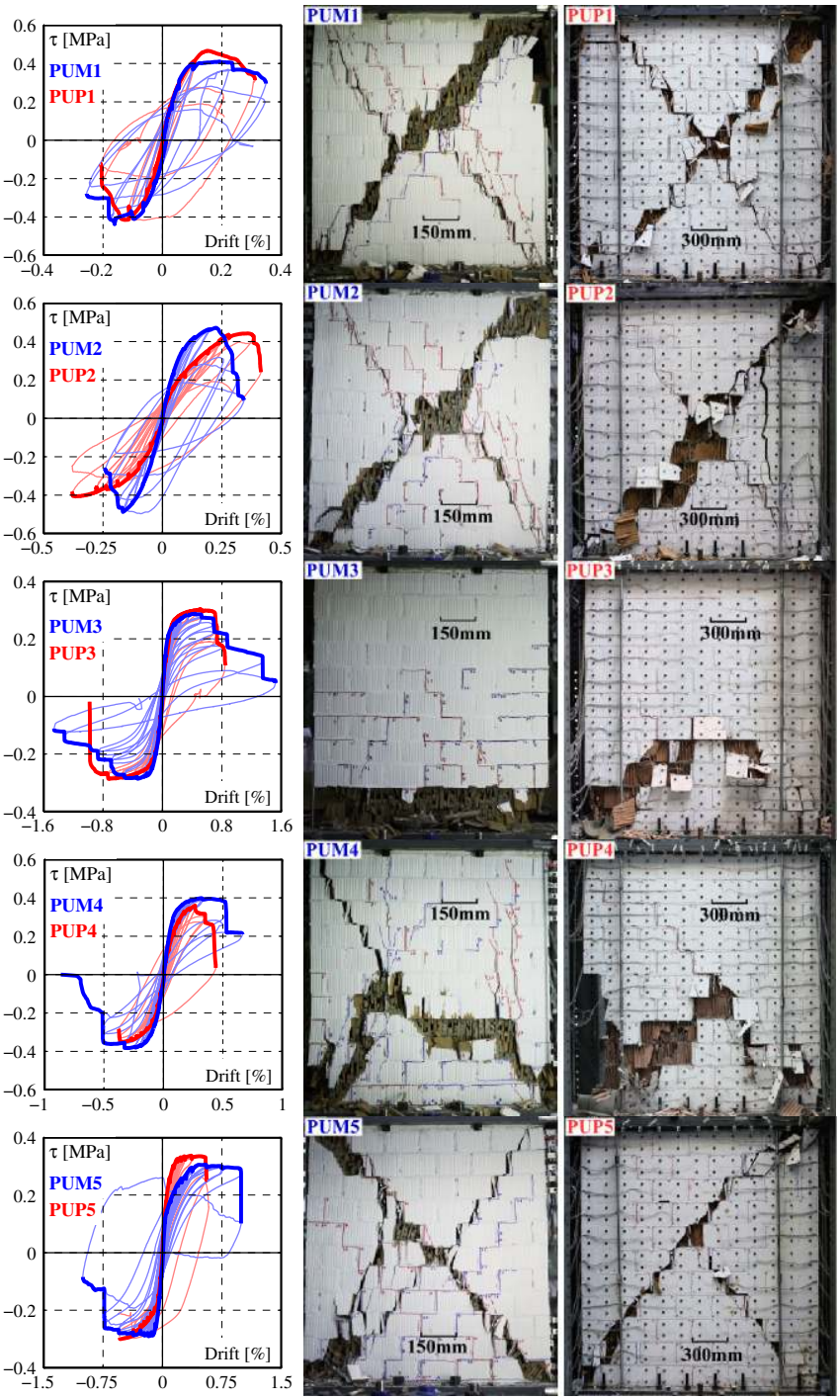

Fig. 8 Comparison of the results from the quasi-static tests on the half-scale (PUM1-5) and the full-scale masonry walls (PUP1-5): hysteresis loops with envelopes (*left*) and damages of the photo of the walls after axial load failure (*centre*: half-scale, *right*: full-scale)

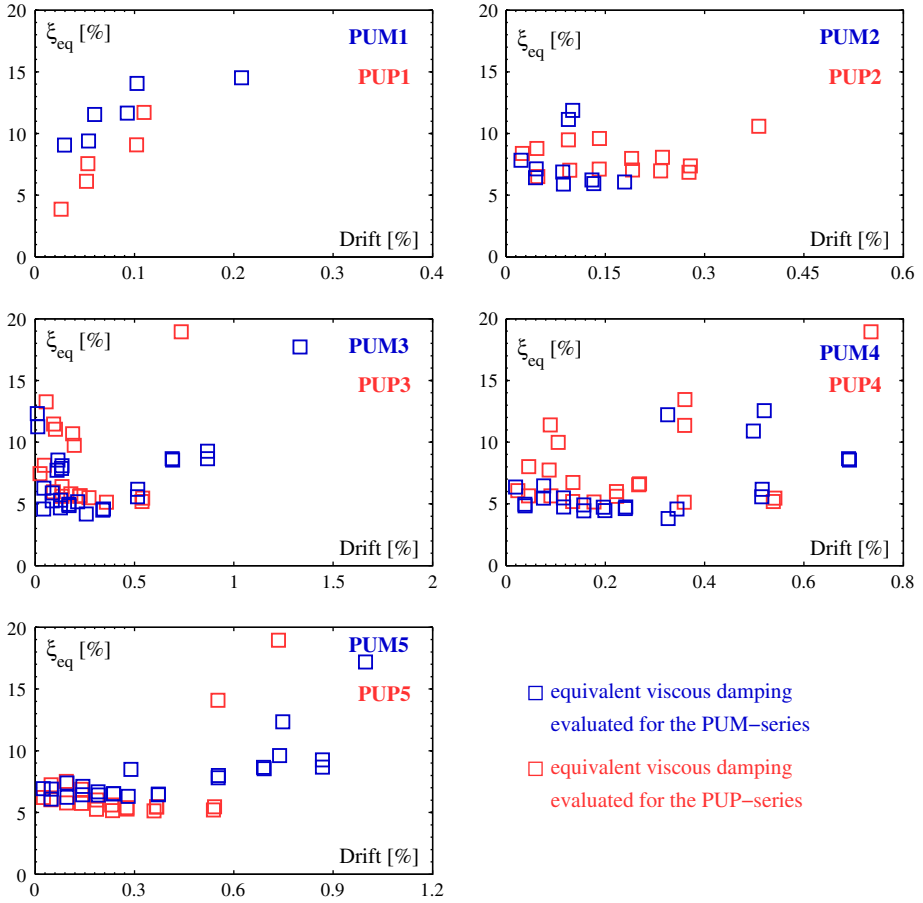

Fig. 9 Comparison of equivalent viscous damping ratios; The equivalent viscous damping ratios are evaluated according to Magenes and Calvi (1997)

significant for PUP1 than for PUM1, resulting therefore in very similar drift capacities for the two walls. For PUM1, the vertical pistons were controlled to keep the shear span constant at $0.5H$. This resulted in very small rotations of the top beam in the post peak branch. Nevertheless, these rotations were very small and are neglected in the following discussion.

In general, horizontal and diagonal cracks tended to appear later in the half-scale walls than in the full-scale walls. Especially at small drifts—when the walls behaved still largely in an elastic manner—the crack opening was generally smaller in the half-scale walls than in the full-scale walls and it seemed to the authors that the crack width was scaled accordingly to the scaling of joints and bricks. Thus, the initial cracks in the half-scale walls were simply too small to be detected at the same stage as the full-scale walls and onset of cracking was observed later in the half-scale walls. For PUM5/PUP5, the first diagonal cracks were noticed at the same nominal drift of 0.15 %. However, even though throughout the testing the crack formation was similar, the cracks appeared generally at more important drifts for PUM5. In the walls where flexural deformations contributed in a significant manner to the total deformations—PUM3/PUP3, PUM4/PUP4 and PUM5/PUP5—the horizontal cracks

developed generally later in the half-scale walls than in the full-scale walls. Nevertheless, the delay of the onset of horizontal cracking was less than for diagonal cracking and might thus explain why PUM4 displayed a stronger rocking behaviour than PUP4.

This observation is also confirmed by the crack widths, which we determined from the optical measurements. Figure 10 shows the 98 %-fractile value of the crack widths ($w_{ver,M}$ and $w_{ver,P}$ refer to vertical cracks which developed through bricks or head joints and $w_{hor,M}$ and $w_{hor,P}$ to the horizontal crack width measured in bed-joints). The 98 %-fractile value is determined for all locations of potential cracks using the LED-measurements shown in Fig. 6. For all plots the crack opening for the half-scale walls is plotted using the double scale than for the prototype masonry ($2w_{hor,M} = w_{hor,P}$ and $2w_{ver,M} = w_{ver,P}$). Hence, when blue curves and red curves match, the crack width of the model masonry is half the crack width of the prototype masonry and therefore perfectly scaled. The parameters δ_e and δ_u in Fig. 10 represent the elastic and ultimate drift values and refer to the limit of the linear elastic behaviour and the horizontal drift capacity. They will be explained more in detail in the next section. However, it can be noted that for drift demands in the linear-elastic domain ($\delta < \delta_e$), the crack widths of the model masonry tend to be approximately half the crack widths of the prototype masonry. Thus, the measurement confirms the good similitude in the elastic behaviour. For larger drifts, the agreement is slightly less satisfactory and the cracks in the prototype walls tended to be wider than $2w_M$. Hence, for the prototype walls the deformations were concentrated in fewer cracks than in the model masonry.

5.3 Comparison of stiffness, force and displacement capacities

In order to compare the stiffness, force and displacement capacities in more detail, the force-drift envelopes are approximated by bi-linear curves, following the method outlined in Frumento et al. (2009). In this method, the elastic stiffness k_e is estimated as secant stiffness when the force capacity reaches 70 % of the peak force ($0.7V_{max}$). The ultimate displacement Δ_u corresponds to the so-called "horizontal load failure" (see Sect. 5.1) when the force drops to 80 % of the peak strength. The ultimate strength V_u is computed such that the area under the envelope up to ultimate displacement Δ_u is the same as under the bilinear curve. The elastic displacement Δ_e is the intersection point of the elastic branch with stiffness k_e and the horizontal line determined by V_u. In addition to the bi-linear method as applied by Frumento et al. (2009), we determined the maximum displacement Δ_{max} which is associated to the previously defined "axial load failure" (Sect. 5.1). Furthermore, in order to simplify the comparison of the results of the walls at different scales, the displacement and force quantities are replaced by quantities which are independent of the scale, i.e. the interstorey drift $\delta = \Delta/H$ (Δ_e, Δ_u and Δ_{max} change to δ_e, δ_u and δ_{max}) and the mean shear stress $\tau_u = V_u/A$ where H is the height of the wall (see Fig. 7) and A the area of the gross cross section of the wall. The envelopes and the bilinear approximations of all 5 PUM/PUP-pairs are illustrated in Fig. 11.

The characteristic values obtained from the bilinear approximations of the force-displacement envelopes are summarized in Table 7. The table also indicates the compressive strength $f_{c,m}$ of the mortar at the day of the wall tests and the axial stiffness $E_{LS0-LS1}$ of the wall which was computed from the shortening of the wall when applying the axial load at the beginning of each quasi-static cyclic test. Figures 12, 13 and 14 illustrate the ratio of the characteristic properties for each PUM/PUP-pair. In order to compare the walls according to their failure mechanism, in Figs. 12, 13 and 14, the walls are ordered first according to their shear span ($H_0 = 0.5H$, $0.75H$ and $1.5H$) and then according to the axial load ratio ($\sigma_{0,i}$ = 50 % σ_0, 100 % σ_0 and 150 % σ_0).

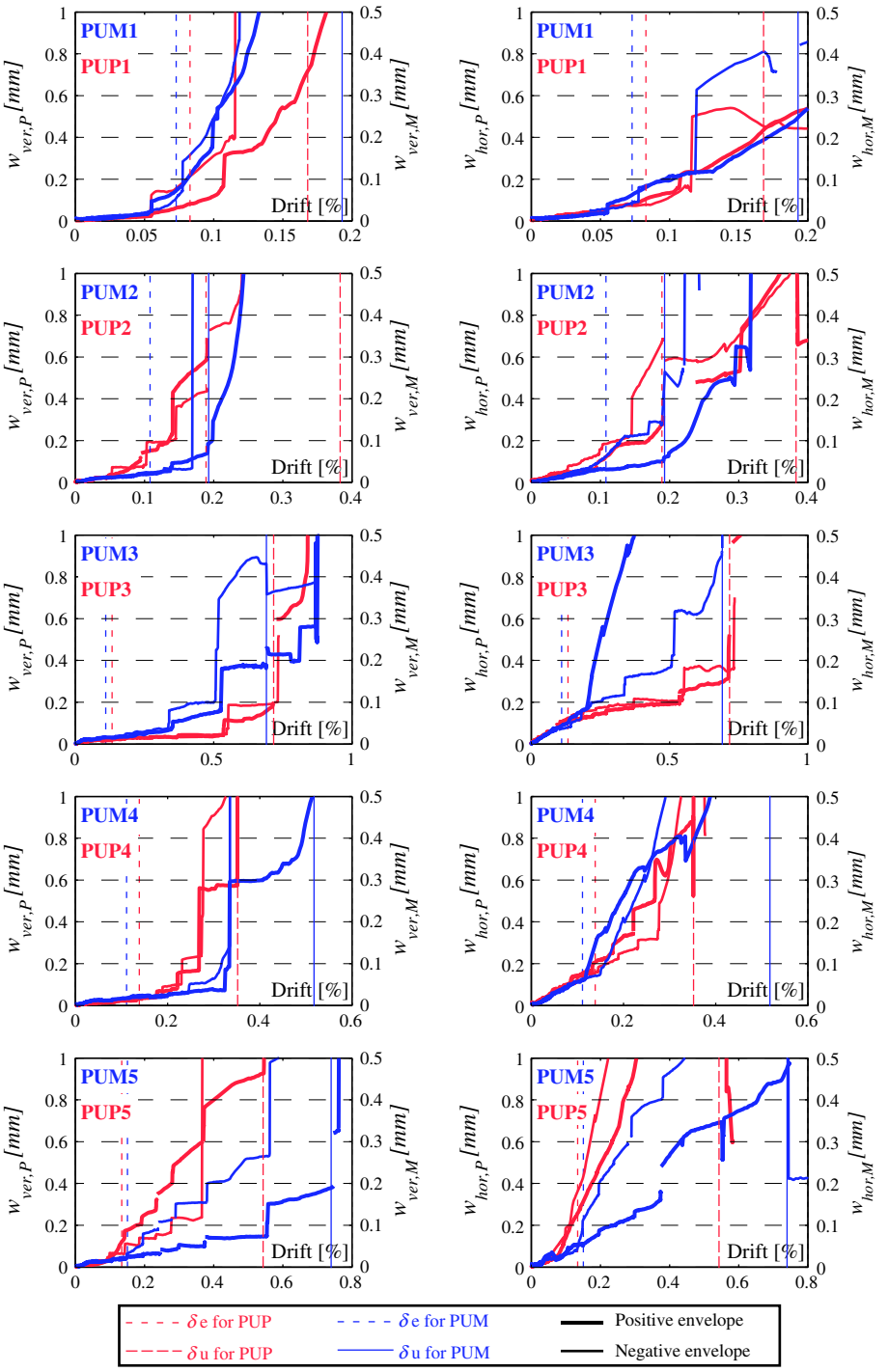

Fig. 10 98 %-fractile of the width of vertical cracks (w_{ver}) in bricks and head joints (indicator for diagonal cracks, at the *left*) and of the width of the horizontal cracks (w_{hor}) in bed joints (indicator for flexural cracking, at the *right*)

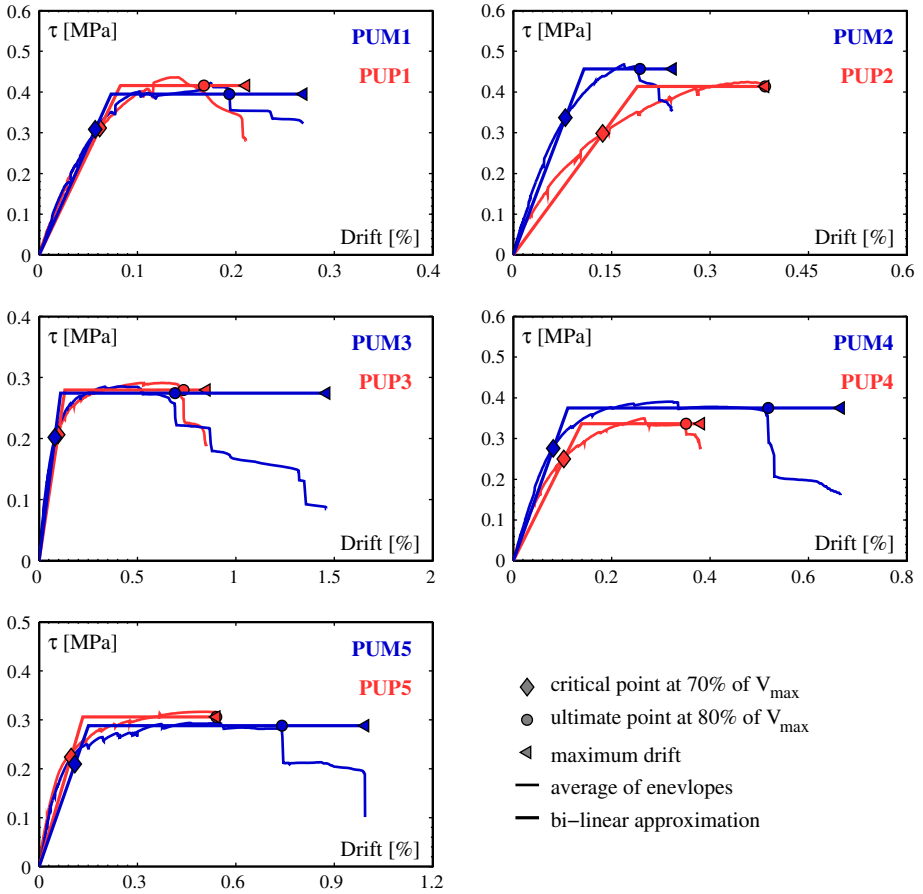

Fig. 11 Mean envelope for PUP1-5/PUM1-5 and resulting bilinear approximation, until horizontal failure and maximum drift at vertical failure

The age of the walls at the day of testing varied between ~40 and 120 days within one series. To obtain similar mortar strength values for the model and prototype walls, each PUM/PUP-pair was tested at a similar age. Even though the mortar strength $f_{c,m}$ showed a slight tendency to increase with age (Table 7), it did not vary significantly within each PUM/PUP-pair and thus did not affect the shear strength similitude of the walls (Fig. 12). For instance, for the first two pairs, PUM1/PUP1 and PUM2/PUP2, the shear strength obtained at half-scale matches perfectly with the one obtained at full-scale (Fig. 12). Due to the larger net area of the model brick, the tensile strength of the model brick was larger than the tensile strength of the prototype brick while the interface strength is smaller for the model brick (see Sects. 4 and 5). The mismatch in net area might therefore change the relative contributions of the different mechanisms to the shear resistance while the total shear strength of the walls remains largely unaffected. In PUM5/PUP5, few cracks developed in the bricks. Cracks through bricks developed only for larger drift demands and these cracks seemed to be caused by geometrical incompatibility when sliding occurs along the joints. Hence, for these walls, the shear strength seems to stem mainly from the sliding mechanism and therefore the full-scale wall is slightly stronger. The pairs PUM3/PUP3 failed due to rocking while PUM4/PUP4

Table 7 Comparison of the characteristic properties of the half- and full-scale walls (resulting material strength in bold)

Wall unit	H_0/H (−)	σ_0/f_u (−)	Failure mode	δ_e (%)	δ_u (%)	δ_{max} (%)	τ_u (MPa)	k_e (kN/m^2)	$f_{c,m}$ (MPa)	$E_{LS0-LS1}$ (GPa)
PUP1	0.5	0.18	**S**	**0.083**	**0.168**	**0.210**	**0.416**	**50.3**	**8.99**	**4.86**
PUM1	0.5	0.18	**S**	**0.073**	**0.193**	**0.268**	**0.395**	**53.8**	**9.27**	**6.03**
Ratio 1	–	–	–	0.89	1.15	1.28	0.95	1.07	1.03	1.24
PUP2	0.75	0.18	**S**	**0.189**	**0.383**	**0.383**	**0.413**	**21.8**	**9.75**	**4.05**
PUM2	0.75	0.18	**S**	**0.108**	**0.193**	**0.243**	**0.456**	**42.3**	**11.3**	**11.7**
Ratio 2	–	–	–	0.57	0.50	0.63	1.10	1.94	1.16	2.89
PUP3	1.5	0.18	**F**	**0.133**	**0.717**	**0.843**	**0.280**	**21.0**	**12.0**	**3.05**
PUM3	1.5	0.18	**F**	**0.110**	**0.691**	**1.459**	**0.274**	**25.0**	**12.3**	**3.70**
Ratio 3				0.82	0.96	1.73	0.98	1.19	1.03	1.21
PUP4	1.5	0.26	**H**	**0.139**	**0.352**	**0.382**	**0.336**	**24.2**	**11.7**	**4.05**
PUM4	1.5	0.27	**H**	**0.111**	**0.518**	**0.665**	**0.375**	**33.8**	**9.45**	**7.58**
Ratio 4				0.80	1.47	1.74	1.12	1.40	0.81	1.87
PUP5	0.75	0.09	**S**	**0.134**	**0.543**	**0.546**	**0.306**	**22.9**	**9.87**	**4.94**
PUM5	0.75	0.10	**S**	**0.151**	**0.740**	**0.993**	**0.288**	**19.1**	**11.9**	**11.6**
Ratio 5				1.13	1.36	1.82	0.94	0.83	1.21	2.35
Average ratio				0.84	1.09	1.44	1.02	1.29	1.05	1.91

developed a mixed failure mode. Compression tests on model and prototype masonry showed that the compressive strengths f_u were very similar (Table 3) and consequently for both pairs the similitude of strength between model and prototype walls is excellent (Fig. 12).

The axial stiffness $E_{LS0-LS1}$ of the model masonry is in average larger than the axial stiffness of the prototype masonry (Fig. 13). In the case of PUM2/PUP2, the difference in axial stiffness amounts to more than 150 % while the average ratio of axial stiffness for the model to prototype walls is 1.9. When neglecting the pair PUM2/PUP2, the agreement of the elastic horizontal stiffness k_e between model and prototype wall depends on whether the wall is developing a shear or rocking behaviour: For walls developing a shear failure mode (PUM1/PUP1 and PUM5/PUP5), the agreement of the stiffness is better than for walls with a hybrid (PUM4/PUP4) or rocking failure mode (PUM3/PUP3); for the latter the horizontal stiffness of the model walls is in average 30 % larger than the stiffness of the prototype walls. This is in agreement with findings from the material tests where the E-modulus of the half-scale masonry exceeded the E-modulus of the full-scale masonry by ∼50 % (Table 3).

Figure 14 shows the ratios of the drift capacities of the model and prototype walls. As previously noted, the similitude of the elastic drift δ_e is generally good. The drift capacity associated with horizontal load failure is in average 9 % larger for the model walls than for the prototype walls. The drift δ_{max} at vertical failure is for all model walls (with the exception of PUM2) larger than for the corresponding prototype walls. The average ratio of the drifts δ_{max} is 1.44. Our observation of an increased displacement capacity in the post peak branch agrees hence with the observation done by Hendry and Sinha (1971). However, in Fig. 15 the drift capacity is plotted following the approach of Petry and Beyer (2014) in dependency of the boundary conditions—shear span ratio and axial stress ratio—and it can be noted that generally a good similitude is obtained for the elastic and ultimate drift. At axial load failure the model walls tend to have a significant higher maximum drift capacity (Figs. 14, 15).

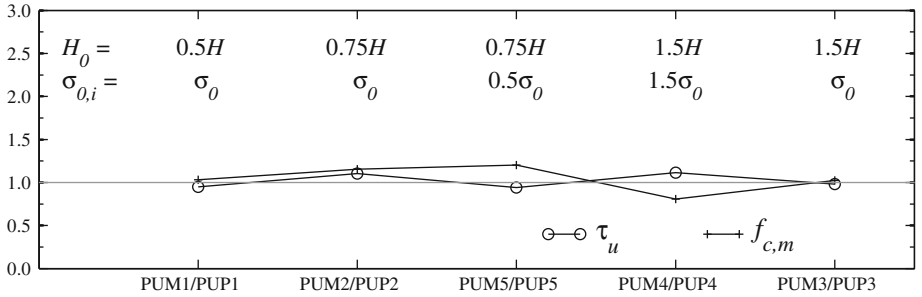

Fig. 12 PUM/PUP ratio of the shear capacity τ_u and of the compressive strength $f_{c,m}$ of the corresponding mortar cubes

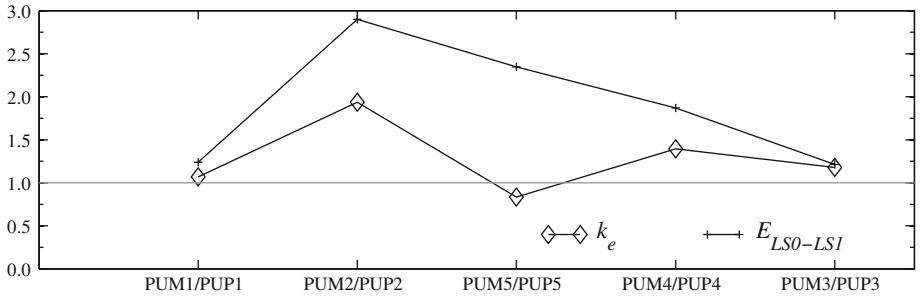

Fig. 13 PUM/PUP ratio of the initial stiffness k_e and of the measured axial stiffness $E_{LS0-LS1}$ during the first axial load application from LS0 to LS1

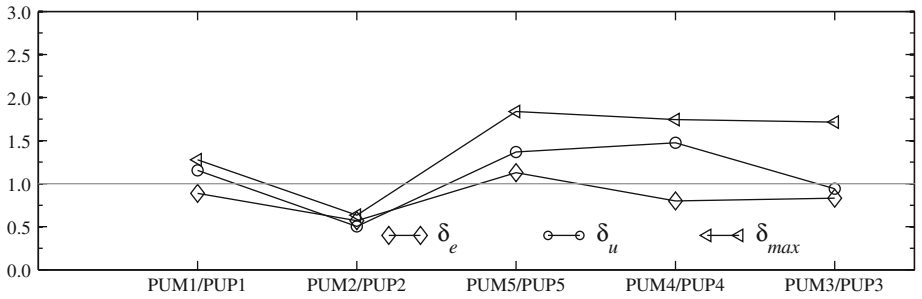

Fig. 14 PUM/PUP ratio of the drift capacities δ_e, δ_u and δ_{max}

6 Conclusions

Shake table tests of entire buildings often require testing at a reduced-scale. This paper provides guidelines for the scaling of modern unreinforced masonry buildings with hollow clay brick units. Based on the results of tests on brick units, standard material tests and quasi-static cyclic tests on walls, we recommend the following geometry for a model hollow clay brick unit:

- Similar absolute web and shell thicknesses as the prototype brick,
- Similar void ratio and similar effective width of webs and shells as the prototype brick (ratio of the sum of the web and shell thicknesses to the total width of the bricks),

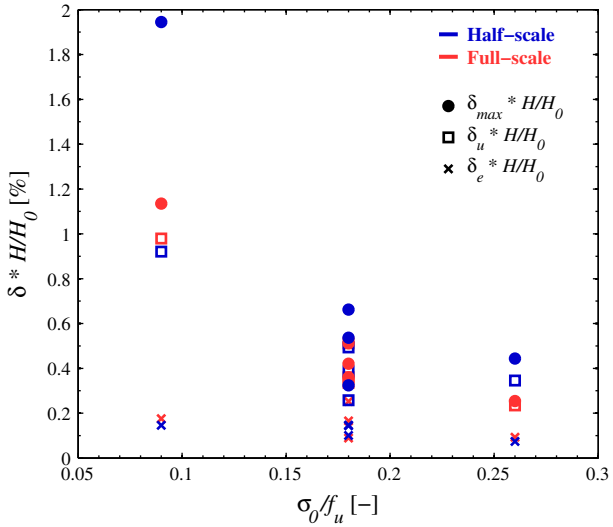

Fig. 15 Comparison of the displacement capacities δ_e, δ_u and δ_{max} in dependency of the boundary conditions (axial stress ratio σ_0/f_u and shear span ratio H_0/H)

- Similar layout of the hole pattern as the prototype brick (e.g. rectangular webs with straight, continuous webs vs. rice-shaped holes).

The model brick should be produced from the same clay as the prototype brick. Since the web and shell thicknesses are similar to those of the prototype brick, it should be dried and burnt using the same procedure as for the prototype brick. The bricks should be wire-cut before the burning in order to obtain similar mortar-brick interface properties as for the prototype masonry.

It is clear that such scaling of the brick is restricted to rather moderate scaling factors. In this study, masonry at half- and full-scale was compared. Using these guidelines, we obtained an excellent match of the bricks' compressive strengths in the vertical and horizontal direction. Comparison of the results from standard material tests on brick units and masonry wallettes as well as results from quasi-static cyclic tests on walls indicate further:

- Due to the excellent match in brick strength, also the compressive strengths of the masonry at half- and full-scale are very similar. As a result, the flexural capacity of the walls is well reproduced. The axial stiffness of the model and prototype masonry differed by almost a factor of two. However, the horizontal elastic stiffnesses of the walls were rather similar. Previous studies suggested that the different axial stiffnesses are caused by the different overburden pressures during curing of the mortar.
- The net areas of the model and prototype brick units used in this study differed by 20 %. As a result the interface shear strength of the model masonry was 20 % lower and the tensile brick strength 27 % higher than for the prototype masonry. The shear strength of the walls was, however, not that different indicating that in most cases both resisting mechanisms contributed to the shear strength of the wall. The differences in net brick areas were due to the fact that (i) the web and shell thicknesses were identical for the model and prototype brick and (ii) an existing form of a full-scale brick unit was modified rather than a new form designed for the model brick. If a new form is designed for the model brick, it is suggested to aim for a slightly reduced net area of the brick by reducing

slightly the web and shell thickness. This should increase the interface shear strength of the model masonry and reduce the tensile strength of the brick. Hence, such a model brick is expected to yield an even improved similitude between model and prototype masonry.

- The least satisfying match between half- and full-scale masonry was obtained with regard to the drift capacities at axial load failure. While the ultimate drift capacity associated with horizontal load failure corresponds still rather well between model and prototype masonry (average difference of 9 %), the drift capacities associated with axial load failure were significantly larger for the half-scale masonry than for the full-scale masonry. This is most likely related to size effects that can lead to larger deformation capacities of small-scale specimens than for full-scale specimens. The results suggest that the proposed scaling of the masonry did not reduce the fracture energy associated with the compression failure of the masonry correctly. At present, mechanical models that link material properties to ultimate wall drifts are missing. In addition, standard material tests address only the strength and not the deformation capacity of masonry. Such models and tests would be necessary in order to estimate already on the material test level, whether a similar drift capacity of the walls at reduced- and full-scale can be expected. Existing empirical models only consider the slenderness ratio and the failure mode, which was always correctly reproduced. Once mechanical models for the drift capacity are available it might be possible to refine the recommendations for the scaling of masonry.

Which of the above properties is the most important property to be matched, depends of course on the objectives of the reduced-scale test that is to be conducted and on the limit states to be addressed. If, for example, only limit states up to the "Significant Damage" limit state (CEN 2004) are addressed, the difference in drift capacity associated with axial load failure might be of lesser importance as the behavior up to peak strength and even up to horizontal load failure (20 % drop in peak strength) is rather well reproduced by the model masonry.

Acknowledgments The authors thank the two reviewers for their comments that helped improving the manuscript. The authors would also like to thank Morandi Frères SA and in particular Philip Piguet, Switzerland, for the effort put into the production of the small-scale bricks and for the donation of the small- and full-scale bricks. Thanks also to Salvatore Marino for his help during testing of the reduced-scale walls.

References

Abrams DA (1996) Effects of scale and loading rate with tests of concrete and masonry structures. Earthq Spectra 12(1):13–28

Benjamin JR, Williams HA (1958) The behavior of one-story brick shear walls. J Struct Div, Proceedings of the American Society of Civil Engineers, Proc. Paper 1723: 1–30

Brocken HJP, Spielmann ME, Pel L, Kopinga K, Larbi JA (1998) Water extraction out of mortar during brick laying: a NMR study. Mater Struct 31:49–57

CEN (2002) EN 1052–1: Methods of test for masonry—part 1: determination of compressive strength. European Committee for Standardisation, Brussels, Belgium

CEN (2004) Eurocode 8: Design of structures for earthquake resistance—part 3: strengthening and repair of buildings EN 1998–3:2004. European Committee for Standardisation, Brussels, Belgium

CEN (2005) Eurocode 6: Design of masonry structures—part 1–1: general rules for reinforced and unreinforced masonry structures EN 1996-1-1:2005. European Committee for Standardisation, Brussels, Belgium

CEN (2007) EN 1052–3: Methods of test for masonry—part 3: determination of initial shear strength. European Committee for Standardisation, Brussels, Belgium

Davies M, Hughes T, Taunton P (1995) Considerations in the small scale modelling of masonry arch bridges. In: Arch bridges. Thomas Telford, London, pp 365–374

Drysdale RG, Hamid AA (2008) Masonry structures: behavior and design, 3rd edn. The Masonry Society, Boulder

Egermann R, Cook D, Anzani A (1991) An investigation into the behaviour of scale model brick walls. In: Proceedings of the ninth international Brick/Block Masonry conferences. Berlin, Germany, pp 628–635
Frumento S, Magenes G, Morandi P, Calvi GM (2009) Interpretation of experimental shear tests on clay brick masonry walls and evaluation of q-factors for seismic design. IUSS Press, Pavia
Ganz HR (1985) Mauerwerksscheiben unter Normalkraft und Schub. Dissertation, ETH Zürich, Switzerland
Green K, Carter M, Hoff W, Wilson M (1999) The effects of lime and admixtures on the water-retaining properties of cement mortars. Cem Concr Res 29(11):1743–1747
Hamid AA, Abboud B, Harris HG (1986) Direct small scale modeling of grouted concrete block masonry. In: U.S.-PRC joint workshop on seismic resistance of masonry structures. Harbin, China
Hendry AW, Murthy CK (1965) Comparative tests on 1/3- and 1/6-scale models brickwork piers and walls. In: Proceedings of the British Ceramic Society, No. 4, pp 44–66
Hendry AW, Sinha BP (1971) Shear tests on full-scale single-storey brickwork structures subjected to pre-compression. J. Civil Eng. Public Works Rev. pp 1339–1344
Krawinkler H (1979) Possibilities and limitations of scale-model testing in earthquake engineering. In: Proceedings of the second US national conference on earthquake engineering. Stanford, California, pp 283–292
Lourenço PB, Vasconcelos G, Medeiros P, Gouveia J (2010) Vertically perforated clay brick masonry for loadbearing and non-loadbearing masonry walls. Constr Mater 24(11):2317–2330
Lourenço PB (1997) Two aspects related to the analysis of masonry structures: size effect and parameter sensitivity. Technical report, TU-DELFT No 03.21.1.31.25/ TNO-BOUW No 97-NM-R1533, Faculty of Engineering, TU Delft, Netherlands
Magenes G, Calvi GM (1997) In-plane seismic reponse of brick masonry walls. Earthq Eng Struct Dyn 26:1091–1112
Mohammed A (2006) Experimental comparison of brickwork behaviour at prototype and model scales. Dissertation, Cardiff University, UK
Mohammed A, Hughes T (2011) Prototype and model masonry behaviour under different loading conditions. Mater Struct 44(1):53–65
Petry S, Beyer K (2014) Influence of boundary conditions and size effect on the drift capacity of URM walls. Eng Struct 65:76–88
RILEM (1991) RILEM TC 76-LUM: Diagonal tensile strength tests of small wall specimens. RILEM Publications SARL
Shrive NG, Jessop EL (1980) Anisotropy in extruded clay units and its effect on masonry behaviour. In: Proceedings of the 2nd Canadian masonry symposium, Ottawa, pp 39–50
Sinha BP, Hendry AW (1969) Racking tests on storey-height shear-wall structures with openings subjected to precompression. Designing, engineering and constructing with masonry products, Gulf Publication Co., Houston, Texas, pp 192–199
Tomaževič M (1987) Dynamic modelling of masonry buildings: storey mechanism model as a simple alternative. Earthq Eng Struct Dyn 15(6):731–749
Tomaževič M, Weiss P, Velechovsky T, Modena C (1990) Seismic behaviour of masonry buildings—shaking-table study of masonry buildings with different structural configuration— summary report, models 1,2,3 and 4. Test report, Ministry of Research Activity and Technology, Ljubljana, Slovenia
Tomaževič M, Velechovsky T (1992) Some aspects of testing small-scale masonry building models on simple earthquake simulators. Earthq Eng Struct Dyn 21(11):945–963